ARCHIVE OF MECHANICAL ENGINEERING

DOI: 10.24425/ame.2025.153738 2025, Vol. 72, No. 1, pp. 85–103

Michał MODZELEWSKI [1], Piotr LICHOTA [1]

Analysis of wavelet transform application in aircraft longitudinal motion identification

Received 14 October 2024, **Revised** 3 February 2025, **Accepted** 18 February 2025, **Published online** 28 February 2025

Keywords: system identification, wavelet transform, flight dynamics, aeronautics, modelling

This study investigates the application of wavelet transforms in identifying aircraft longitudinal motion dynamics. The Output Error Method, enhanced with wavelet transforms, specifically Haar wavelets at varying decomposition levels, was used to estimate system parameters. The impact of filtering wavelet coefficients and the use of a coherence function in determining parameter changes were analyzed to assess their effect on model identification accuracy. The identification process involved estimating the parameters of a linear model by fitting its responses to those of a nonlinear system, which were noise-perturbed and treated as measurement data. The results demonstrate the successful application of wavelet transforms in system identification for flying objects, with recommendations for further optimization.

1. Introduction

System identification is a methodology for building mathematical models of dynamic systems by using measurements of the system's input and output signals [1]. This process is one of the three main problems associated with the dynamics of any system: simulation, control, and identification [2]. The interconnected nature of these problems highlights the utility of system identification in tasks such as developing models for flight simulators [3], formulating control principles, assessing aerodynamic properties, and validating tunnel test results.

Research on this topic began in the early stages of aviation development. In 1919, H. Glauert published his work on phugoidal motion studies [4], and between 1919 and 1923, F.H. Norton focused on deriving stability derivatives [5]. In 1951, M. Shinbort proposed using the least squares method to determine stability

✉ Michał MODZELEWSKI, email: michal.modzelewski5.dokt@pw.edu.pl

[1] Warsaw University of Technology, Institute of Aeronautics and Applied Mechanics, Poland

derivatives [6], an approach equivalent to the Output Error Method. A significant breakthrough occurred with the widespread adoption of digital computers and the implementation of software for the maximum likelihood method by K.J. Astrom and T. Bohlin in 1965 [7].

Subsequent work on system identification led to the development of various aspects of this methodology. One of the most renowned methods describing the entire identification process is the Quad-M method (Maneuver, Measurement, Methods, Models) [2]. The first two elements of the method refer to planning and conducting measurements during flight campaigns. The last two elements focus on the development of a mathematical model for the studied system.

In the case of identification methods, the most frequently used approaches include the Output Error Method, Equation Error Method, and Filter Error Method. The main classification of methods is the division according to the domain of representation of measurement data used for calculations. The two main domains are time and frequency.

Time-domain methods are easier to interpret and are popular in the identification of both manned aircraft [8] and unmanned aerial vehicles [9], with detailed implementation provided by R.V. Jategaonkar [2]. Frequency-domain methods are more commonly employed for the identification of rotorcraft [10] and in the design of input signals [11], with comprehensive descriptions found in the book by M.B Tischler [12].

However, in recent years, there has been a noticeable trend in flying object identification towards solutions that combine these two domains, such as through the application of wavelet transforms. The wavelet transform is a widely used tool in numerous applications, including image compression [13], medical signal analysis [14], and mechanical fault diagnostics [15]. In the aerospace field, it is applied for flutter prediction [16], automatic maneuver detection [17], fault detection in dynamic systems [18], and system-identification maneuver design [19, 20]. Wavelet transforms have been successfully applied a few times for the identification of transport aircraft [21], spinning projectile [22], unmanned aerial vehicles [23] or flexible aircraft model [24]. Some studies also highlight the potential of combining wavelet transforms with artificial neural networks for system identification [25].

In the aforementioned applications of wavelet transforms for aircraft identification, authors primarily focused on demonstrating the feasibility of using wavelet transforms for successful system identification. This paper provides a deeper analysis of the influence of wavelet transform parameters, such as the decomposition levels and the impact of weighting functions, including coherent and arithmetic mean weighting functions, on the identification results. Although the use of wavelet transforms with coherent weighting functions has been used in [21, 22], the presented results were limited to a single computational case. Additionally, this paper investigates the impact of applying high-pass filtering to wavelet transform coefficients, a topic not addressed in other studies.

The article is organized as follows. At the beginning, the model section describes the non-linear model of longitudinal motion along with the linearization of this model. Then, the designed excitation signal is presented. The next chapter focuses on identification methods. The Output Error Method and the use of wavelet analysis are described. The further parts of the article contain information about the filters and weight functions used for signal processing during identification using the wavelet transform. The next section contains the results of the tests performed. Finally, conclusions are presented.

2. Model

To identify the aircraft's longitudinal channel, a nonlinear simulation model of the F-16 was employed as the reference data source in the identification process. This simulation model is considered reliable, as it has been validated and used in flight simulators [26]. The model's responses to the designed input signals, after adding artificial noise, were treated as the actual aircraft's responses. The use of a complex mathematical model as a reference data source is a common approach in system identification, as it significantly reduces both costs and time during the testing phase of new methods.

The model was then identified as linear. To derive the equations of motion for this linear model, the physical model was simplified to a linear mathematical form, which is discussed in more detail in the subsequent subsection. Several assumptions were made to achieve this:

- The aircraft is a rigid body with six degrees of freedom.
- The aircraft's inertial moments remain constant during flight.
- The object is symmetrical in terms of both geometry and mass distribution along the vertical plane.
- A constant engine thrust is maintained, and the only controlled surface is the elevator.
- The airflow is quasi-steady.
- The atmosphere is stationary.
- The Earth's curvature is neglected, and the gravity field is uniform.

During the analysis, it was assumed that the aircraft operates at an altitude of 10,000 ft with a speed of 502 ft/s.

2.1. Nonlinear model

To determine the dynamic equations of motion, the body-fixed coordinate system $Oxyz$ associated with the aircraft was adopted. The second coordinate system, $Ox_g y_g z_g$ is related to the gravity field acting on the aircraft. Both coordinate system origins were set at the aircraft's center of gravity, and the relationships between the systems are presented in Fig. 1. The figure also illustrates the orientation angles of the aircraft — Euler angles: Φ roll, Θ pitch and Ψ yaw.

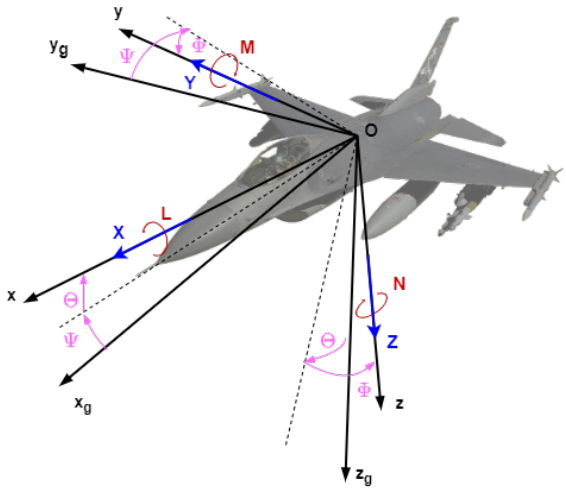

Fig. 1. Coordinates system

The equations of motion were developed from the momentum Π and angular momentum K_O change theorems:

$$\frac{\delta\tilde{\Pi}}{\tilde{\delta t}} + \Omega \times \Pi = F, \tag{1}$$

$$\frac{\delta\tilde{K}_O}{\tilde{\delta t}} + \Omega \times K_O = M_O, \tag{2}$$

where $\Omega = [P, Q, R]^T$ is the angular velocity vector, $F = [X, Y, Z]^T$ and $M_O = [L, M, N]^T$ are external forces and moments vectors and $\frac{\tilde{\delta}}{\tilde{\delta t}}$ denotes the local derivative in the rotating axis system [27]. By making appropriate substitutions, the above equations can be written in matrix form [28]:

$$m\begin{bmatrix}\dot{U}\\ \dot{V}\\ \dot{W}\end{bmatrix} + m\begin{bmatrix}0 & -R & Q\\ R & 0 & -P\\ -Q & P & 0\end{bmatrix}\begin{bmatrix}U\\ V\\ W\end{bmatrix} = \begin{bmatrix}X\\ Y\\ Z\end{bmatrix}, \tag{3}$$

$$\begin{bmatrix}I_{xx} & 0 & -I_{xz}\\ 0 & I_{yy} & 0\\ -I_{xz} & 0 & I_{zz}\end{bmatrix}\begin{bmatrix}\dot{P}\\ \dot{Q}\\ \dot{R}\end{bmatrix} + \begin{bmatrix}0 & -R & Q\\ R & 0 & -P\\ -Q & P & 0\end{bmatrix}\begin{bmatrix}I_{xx} & 0 & -I_{xz}\\ 0 & I_{yy} & 0\\ -I_{xz} & 0 & I_{zz}\end{bmatrix}\begin{bmatrix}P\\ Q\\ R\end{bmatrix} = \begin{bmatrix}L\\ M\\ N\end{bmatrix}, \tag{4}$$

where m is mass of the aircraft, $I_{xx}, I_{yy}, I_{zz}, I_{xz}$ are inertia moments, U, V, W and P, Q, R denotes linear and angular velocities with respect to $Oxyz$ axis.

The forces acting on the aircraft can be divided into components: gravity force $F_g = mg$, aerodynamic force $F_a = [X_a, Y_a, Z_a]^T$, thrust $F_T = [T, 0, 0]^T$. The resultant moment of forces consists of the torque from: gyroscopic forces, aerodynamic forces $M_a = [L_a, M_a, N_a]^T$ and thrust.

Aerodynamic forces and thrust are related to the aircraft's system, in contrast to the gravitational force, which is associated with the Earth's system. To express the gravitational force vector in the $Oxyz$ system, the transformation matrix Λ was used.

$$\Lambda = \begin{bmatrix} 1 & 0 & 0 \\ 0 & \cos\Phi & \sin\Phi \\ 0 & -\sin\Phi & \cos\Phi \end{bmatrix} \begin{bmatrix} \cos\Theta & 1 & -\sin\Theta \\ 0 & 1 & 0 \\ \sin\Theta & 0 & \cos\Theta \end{bmatrix} \begin{bmatrix} \cos\Psi & \sin\Psi & 0 \\ -\sin\Psi & \cos\Psi & 0 \\ 0 & 0 & 1 \end{bmatrix}. \tag{5}$$

By substituting the components of forces and moments into the Eqs. (3)–(4) and using the transformation matrix, the nonlinear equations of motion of aircraft were obtained.

$$\begin{aligned} X_a + T - mg\sin\Theta &= m(\dot{U} + QW - RV), \\ Y_a + mg\sin\Phi\cos\theta &= m(\dot{V} + RU - PW), \\ Z_a + mg\cos\Phi\sin\theta &= m(\dot{W} + PV - QU), \end{aligned} \tag{6}$$

$$\begin{aligned} L_a &= I_{xx}\dot{P} - I_{xz}\dot{R} + (I_{zz} - I_{yy})QR - I_{xz}PQ, \\ M_a - RH_T &= I_{yy}\dot{Q} + (I_{xx} - I_{zz})PR + I_{xz}(P^2 - R^2), \\ N_a + QH_T &= I_{zz}\dot{R} - I_{zx}\dot{P} + (I_{yy} - I_{xx})PQ + I_{xz}QR. \end{aligned} \tag{7}$$

To determine the derivatives of the aircraft's spatial orientation angles, kinematic equations linking changes in Euler angles to the components of the object's angular velocity were used.

$$\begin{aligned} \dot{\Phi} &= P + Q\sin\Phi\tan\Theta + R\cos\Phi\tan\Theta, \\ \dot{\Theta} &= Q\cos\Phi - R\sin\Phi, \\ \dot{\Psi} &= \frac{Q\sin\Phi + R\cos\Phi}{\cos\Theta}. \end{aligned} \tag{8}$$

2.2. Linear model

To linearize Eqs. (6)–(8), small perturbation theory was used [29]. It is assumed that at the equilibrium point, the aircraft's flight is steady, rectilinear and symmetrical. Since the longitudinal motion is analyzed in this paper, the change in the aircraft's elevator deflection δ_E was used as the perturbation introduced into the system. The linearized system of equations for the longitudinal channel is represented as:

$$\begin{aligned}
\dot{u} &= X_u u + X_w w + X_q q - g\theta + X_{dE}\delta_E, \\
\dot{w} &= Z_u u + Z_w w + Z_q q + Z_{dE}\delta_E, \\
\dot{q} &= M_u u + M_w w + M_q q + M_{dE}\delta_E, \\
\dot{\theta} &= q.
\end{aligned} \tag{9}$$

In the above equation u, w, q and δ_E represent the perturbations of longitudinal velocity, vertical velocity, pitch angular velocity, and elevator deflection, respectively. The designations X_j, Z_j,M_j adopted in the formulas are the stability and control derivatives for the longitudinal force, vertical force and pitching moment, respectively, and are defined below. The subscripts j appearing next to the derivatives refer to a specific flight parameter or control surface.

$$X_j = \frac{1}{m}\frac{\delta X}{\delta j}, \qquad Z_j = \frac{1}{m}\frac{\delta Z}{\delta j}, \qquad M_j = \frac{1}{I_{yy}}\frac{\delta M}{\delta j}. \tag{10}$$

During the simulation, calculations were initialized for the aircraft in equilibrium. The values of state and control vectors in this state are shown in the following Table 1. The calculations were conducted with respect to changes around the equilibrium point, however, the final results (see Fig. 6 in Section 5) are presented for standard values, which account for the equilibrium point values listed in Table 1.

Table 1. State and control vector values in equilibrium

U [ft/s]	α [deg]	q [deg/s]	θ [deg]	δ_E [deg]
502	0.065	0	0.065	-3.83

3. Input signal

The design of the excitation signal significantly impacts the identification results. When selecting the type of excitation, both multisine signals and various types of rectangular signals were considered [27]. However, the 3-2-1-1 signal was selected for this study due to its effectiveness in providing broad frequency content and its relative simplicity in implementation. This input consists of alternating rectangular pulses with durations in the ratio of 3-2-1-1, creating a wideband signal that is capable of exciting multiple dynamic modes of the aircraft, specifically the longitudinal modes such as the short-period and phugoid modes. This makes it well-suited for system identification, as it enhances the accuracy of parameter estimation by capturing a comprehensive range of the system's dynamics.

The structure of the 3-2-1-1 signal is rectangular and shares similarities with the Haar wavelet, which is employed later in the identification process. Both signals feature abrupt transitions, facilitating the capture of changes in the system's response and potentially improving the coherence between the excitation signal and the identification method.

In addition to its broad frequency coverage, the 3-2-1-1 signal is relatively easy to implement in flight tests, which reduces the risk of errors during execution. Given its balanced combination of simplicity and effectiveness, the 3-2-1-1 input signal is an appropriate choice for identifying the longitudinal dynamics of an aircraft in this study. The elevator deflection signal used in the identification process is shown in Fig. 6.

4. System identification – method

4.1. Output Error Method

The unknown stability and control derivatives were estimated using the Output Error Method (OEM). The OEM is one of the most common identification methods in the time domain. This method is also known as the response curve fitting method. It works by minimizing the error between the measured response and the estimated response value of the mathematical model [2, 27]. Error minimization involves iteratively adjusting parameters of the mathematical model until the desired level of convergence between signals is achieved.

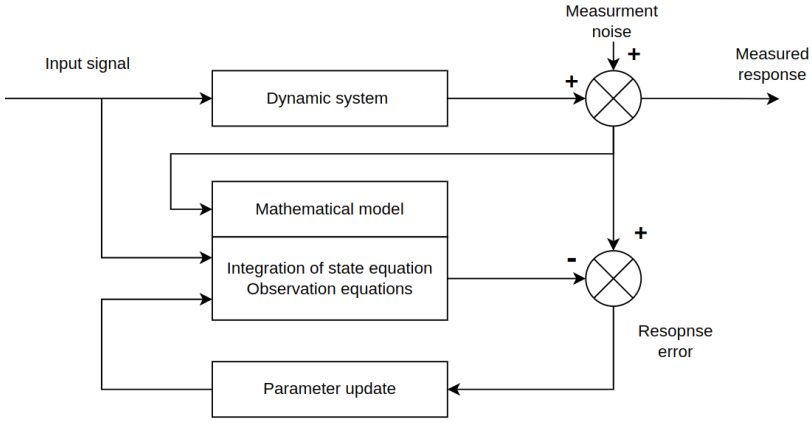

Fig. 2. Block schematic of the Output Error Method [2]

The OEM's implementation is based on Maximum Likelihood Estimation (MLE). The objective of using the MLE is to estimate a model parameters vector Θ for which the probability p of observing the measurements was the highest. As the algorithm iterates, it progressively reduces the difference between the measurements and response of a mathematical model system, leading to increasingly accurate results.

$$\hat{\Theta} = \arg\max_{\Theta} p(z|\Theta), \tag{11}$$

where z denotes the measured response, Θ are model parameters, hat symbol stands for the estimates and $p(z|\Theta)$ is the probability of z given Θ.

Due to the exponential characteristics of many density functions, the logarithm of the likelihood function, sharing the same optimal solution, is typically preferred. Consequently, the maximum likelihood estimate is acquired as such:

$$\hat{\Theta} = \arg\{\min_{\Theta} \ln p(z|\Theta)\}. \tag{12}$$

Assuming that the function $p(z|\Theta)$ is twice differentiable, finding the optimal parameters using the maximum likelihood method comes down to the following equation.

$$\frac{\partial \ln(p(z|\Theta))}{\partial \Theta} = 0. \tag{13}$$

The probability density function for multi-channel response systems, described with N discrete time steps, can be expressed in the form of the following equation.

$$p(z_1, \ldots z_N|\Theta) = \left(\sqrt{(2\Pi^n)}\sqrt{|R|}\right)^{-N/2} \exp\left(-\frac{1}{2}\sum_{k=1}^{N}[z(t_k)-y(t_k)]^T R^{-1}[z(t_k)-y(t_k)]\right) \tag{14}$$

where y is the response vector of the system at a given moment k, and R is the measurement covariance matrix, expressed as:

$$R = \frac{1}{N}\sum_{k=1}^{N}[z(t_k) - y(t_k)][z(t_k) - y(t_k)]^T. \tag{15}$$

The solution of the Eq. (13) can be reduced to minimizing the objective function J. By substituting the measurement covariance matrix into Eq. (14) and neglecting the constant terms, the cost function can be reduced to the following form.

$$J(\Theta) = |R|. \tag{16}$$

During optimization, the estimates and the measurement noise covariance matrix influence each other. To manage this interdependence, a relaxation strategy is applied. This involves alternately optimizing the cost function with respect to the covariance matrix or the estimates, while holding the other constant. The process continues until the results stabilize and converge.

4.2. Wavelet transform

The wavelet transform is a transformation similar to the Fourier transform, with the distinction that instead of sinusoidal functions, it employs functions known as wavelets as the basis of this transformation. The wavelet transform can be

understood as the representation of the original signal as a sum of wavelets, which are tailored to the signal by adjusting two parameters: scaling parameter a and position parameter b. This approach allows the transformation to serve as a tool for simultaneous analysis in both the frequency and time domains [30].

$$\Psi_{a,b}(t) = \frac{1}{\sqrt{a}}\Psi\left(\frac{t-b}{a}\right), \tag{17}$$

where Ψ is the basic wavelet function.

In numerical analysis using wavelets, a primary tool used is the discrete wavelet transform, which allows the decomposition of the signal into different frequency bands while maintaining information about the location of wavelets in the time domain. However, the accuracy of localizing a wavelet at a given frequency band is associated with uncertainty, referred to as Heisenberg's uncertainty principle [31].

The algorithm for discrete wavelet transformation was proposed by S. Mallat and is based on multiresolution analysis. This algorithm can be understood as a group of two types of filters (Fig. 3): high-pass and low-pass filters, which divide the signal into low-frequency components (approximation) and high-frequency components (detail). The response of the low-pass filter can undergo further filtration by high-pass and low-pass filters, to perform the next level of signal division into low and high-frequency components. This procedure can be repeated multiple times, and the number of high-pass and low-pass filtrations is referred to as the decomposition level. The scheme of this decomposition is often called the Mallat's tree.

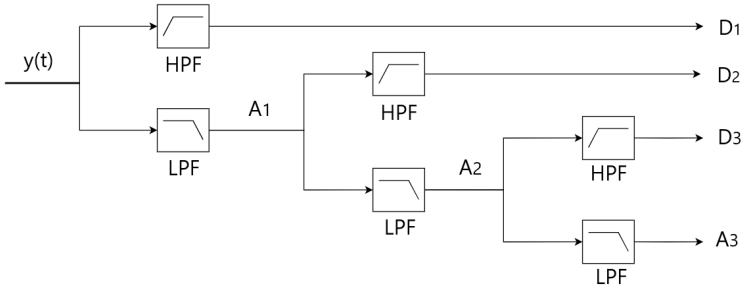

Fig. 3. Schematic diagram of wavelet decomposition – Mallat's tree

The outcome of discrete wavelet transformation is a set of coefficients A_i and D_i describing the components of the signal, representing approximation and detail, where i denotes the level of signal decomposition.

In conducting the decomposition, the Haar wavelet was selected for its effectiveness in extracting information regarding object dynamics based on time histories of aircraft rigid body flight mechanic states [21, 22]. The Haar wavelet, like most wavelets, consists of two functions: the scaling function Φ, used for approximation, and the wavelet function Ψ, utilized to describe detail (Fig. 4).

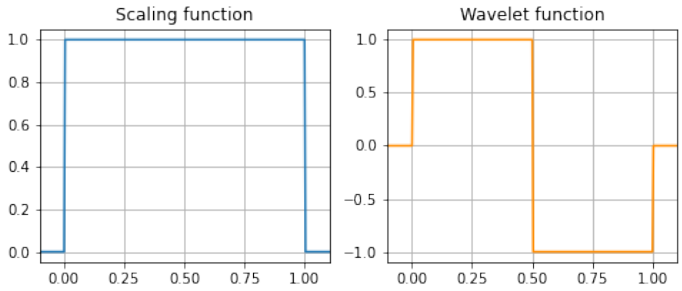

Fig. 4. Haar wavelet

In this work, wavelet analysis has been used to decompose the response of the identified system. The decomposition enables the extraction of coefficients that describe the signal in different frequency bands. The primary goal of this decomposition is to separate the signal into components corresponding to various frequency ranges. This allows for the isolation of components resulting from the aircraft's oscillations from those caused by, for example, measurement noise, sensor drift, or engine vibrations. By applying an inverse discrete transformation, it is possible to reconstruct these individual signal components and analyze them separately, providing deeper insight into the underlying dynamics of the system.

An example of the decomposition and reconstruction of the components of the system's response to the input signal (described in Section 3) is shown in Fig. 5.

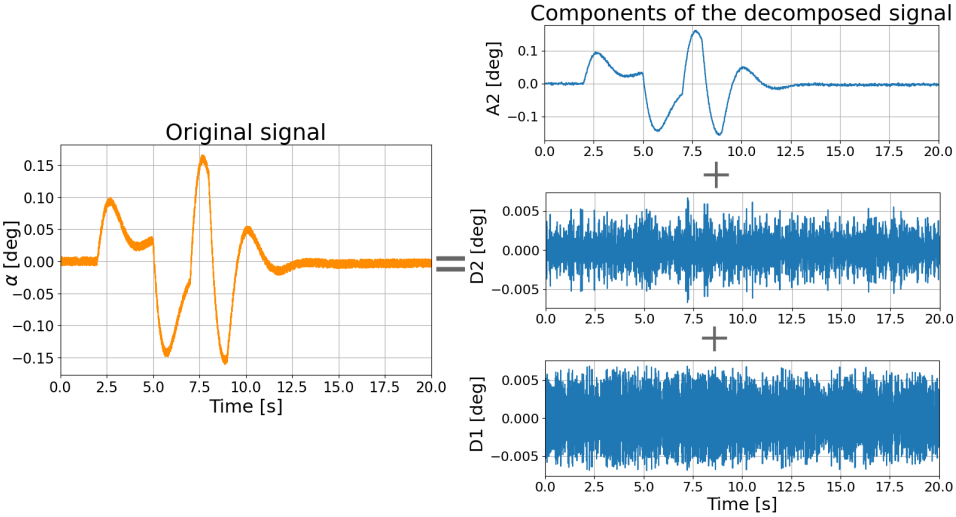

Fig. 5. Example of decomposition and reconstruction of system's response (angle of attack) to the input signal – 2nd level of decomposition

This decomposition into component signals allows the identification algorithms to be used on given components in given frequency bands. This means that during a single iteration of the algorithm for identification, a parameter change vector is determined for each frequency band. Therefore, with a decomposition level of 7 (8 components), 8 vectors of changes in the system parameters are obtained. From these vectors, it is possible to determine the resultant parameter change vector $\Delta\Theta$, which will be used to determine the new system parameters. The formula for calculating the vector $\Delta\Theta$ is shown below.

$$\Delta\Theta = c_{An}\,\Delta\Theta_{An} + \sum_{i=1}^{n} c_{Di}\,\Delta\Theta_{Di}. \tag{18}$$

In this formula, $\Delta\Theta_{An}$ and $\Delta\Theta_{Di}$ denote the parameter change vectors derived from approximation and detail components, respectively, of the aircraft response signals subjected to an n-level decomposition. The coefficients c_{An} and c_{Di} are weights determined based on the weighting functions described in the following subsection.

4.3. Weight function

When identifying real systems and analyzing measurements, certain signal components are known to constitute noise, potentially compromising the accuracy of the identification results. If specific frequency bands are identified as containing noise, the parameter change vectors from these bands might distort the final identification by leading to an inaccurate resultant vector. To address this, a weighting function can be applied to determine the weights (c_{An} and c_{Di}) from Eq. (18) for calculating the resultant parameter change vector $\Delta\Theta$.

As this article focuses on the analysis of the application of wavelet transforms in system identification, two types of weighting functions were employed to determine the resultant parameter change vector. The first approach uses an arithmetic mean, assigning equal weight to each parameter change vector. Another approach is to use a weighted average, where the weights are selected based on signal analysis. In this study, wavelet transformations were tested at the 3rd and 7th levels of decomposition. The signal sampling rate was 256 Hz, which means that the decomposed signal components are in the intervals shown in Table 2.

Table 2. Frequency bands for the 3rd and 7th level of decomposition

Components 3rd level of decomposition	A3					D3	D2	D1
Components 7th level of decomposition	A7	D7	D6	D5	D4	D3	D2	D1
Frequency band [Hz]	0-1	1-2	2-4	4-8	8-16	16-32	32-64	64-128

For a pilot-controlled aircraft, the frequency range of the system response is typically in the range (0.01; 2.0) Hz [27]. It implies that the detail signals primarily represent measurement noise. Therefore, it was decided that the resultant parameter change vector would be calculated from a weighted average of the parameter change vectors calculated for all signal components. A coherence function [32] was used to determine the weights, which compared the measurements with the mathematical model.

$$C_{xy}(f) = \frac{|G_{xy}(f)|^2}{G_{xx}(f)G_{yy}(f)}, \tag{19}$$

where G_{xy} is the reciprocal spectral density of the signals $x(t)$ and $y(t)$, and G_{xx} and G_{yy} are the spectral density of the signals $x(t)$ and $y(t)$, respectively. C_{xy} is the correlation coefficient, the value of which is always in the range $\langle 0; 1 \rangle$.

Determining the weights involves calculating a vector of mean coherence coefficients for the relevant frequency bands, followed by normalizing the resulting vector.

4.4. Wavelet coefficients filter

Another way to modify the OEM using wavelet transforms is to apply a high-pass filter to the coefficients obtained from the discrete wavelet transform. This approach is commonly used in image compression and filtering [13]. The method involves sorting all the coefficients of the decomposed components from the discrete wavelet transform and removing those with the smallest values. These coefficients are considered to have minimal impact on the original signal's representation, which allows for signal compression producing a similar signal that occupies less memory or for noise reduction through signal filtering. In this study, the High-Pass Wavelet Coefficients (HPWC) filtering method is used to filter signals. To reconstruct the signal, the filtered coefficients are subjected to an inverse wavelet transform.

5. Results

To evaluate the proposed methods of using wavelet transforms in identification, a series of experiments were conducted in the implemented simulation environment. The identification process involved estimating the parameters of the linear model (Section 2.2) to match its responses to that of the non-linear system (Section 2.1). Additionally, measurement noise, representing 4 percent, was added to the non-linear system responses. The resulting data were then treated as measurement data.

The non-linear model data were obtained using the SIDPAC software module written in MATLAB [26], while the linear model and the rest of the software,

including the identification algorithms, were implemented in Python. Discrete solvers were used for the wavelet transforms as well as for the rest of the software with sampling frequency 256 Hz.

The identification process was carried out for 7 computational cases. For these cases, the following designations were adopted. The first part of the designation indicates the type of wavelet function, and all calculations employed the Haar wavelet. The second part specifies the decomposition level. The third part denotes the type of weighting function used to determine the resultant parameter change vector (E – arithmetic mean, C – coherence function). The fourth part refers to the HPWC filter coefficients (percentage of coefficients retained for use).

A comparison of the measurement data and the responses of the linear systems obtained during the identification is shown in Fig. 6. To compare the results, the integrated differences between the noise-free response of the non-linear model and the obtained responses were calculated and presented in Table 3.

The analysis began with the simplest case, Haar_3_E_100, where the identification was performed using the 3rd decomposition level, the arithmetic mean as the weighting function, and all coefficients from the decomposed signals. The identified system's response closely matched the measurements for α, q, and θ, though larger discrepancies were observed for the velocity U.

To improve the results, the next two cases explored the impact of the HPWC filter, with calculations conducted using filter coefficients of 90 and 80. As shown in Table 3, the HPWC filter significantly reduced the error for velocity U (over twice as much in the case of Haar_3_E_80), with only a slight degradation in the results for θ, and minimal changes for α and q.

The fourth case, Haar_3_C_100, evaluated the use of coherence functions for weighting, without applying the HPWC filter. This case yielded the smallest error for longitudinal velocity, along with strong alignment for α, q, and θ, similar to the previous cases. Analysis of the coherence-based weights indicated a higher emphasis on low-frequency components, which likely contributed to the improved identification accuracy by reducing the impact of measurement noise.

Based on the positive results from the 3rd decomposition level, both the HPWC filter and coherence-based weight function were further tested at the 7th decomposition level, using filter coefficients of 100 (no filtering), 90, and 80. As shown in Table 3, these cases achieved some of the lowest errors for α, q, and θ, but on the other hand, showed some of the largest errors for longitudinal velocity U.

For reference, Table 3 also presents results for the linear model obtained through numerical linearization. While this model shows relatively low error for velocity U, both Haar_3_C_100 and Haar_7_C_100 demonstrate lower overall errors across all responses.

To compare the estimated parameter values across different identification cases, all values were plotted on common charts (Fig. 7). Additionally, reference parameter values (indicated by orange horizontal lines), which represent the stability and control derivatives obtained during numerical linearization, were highlighted.

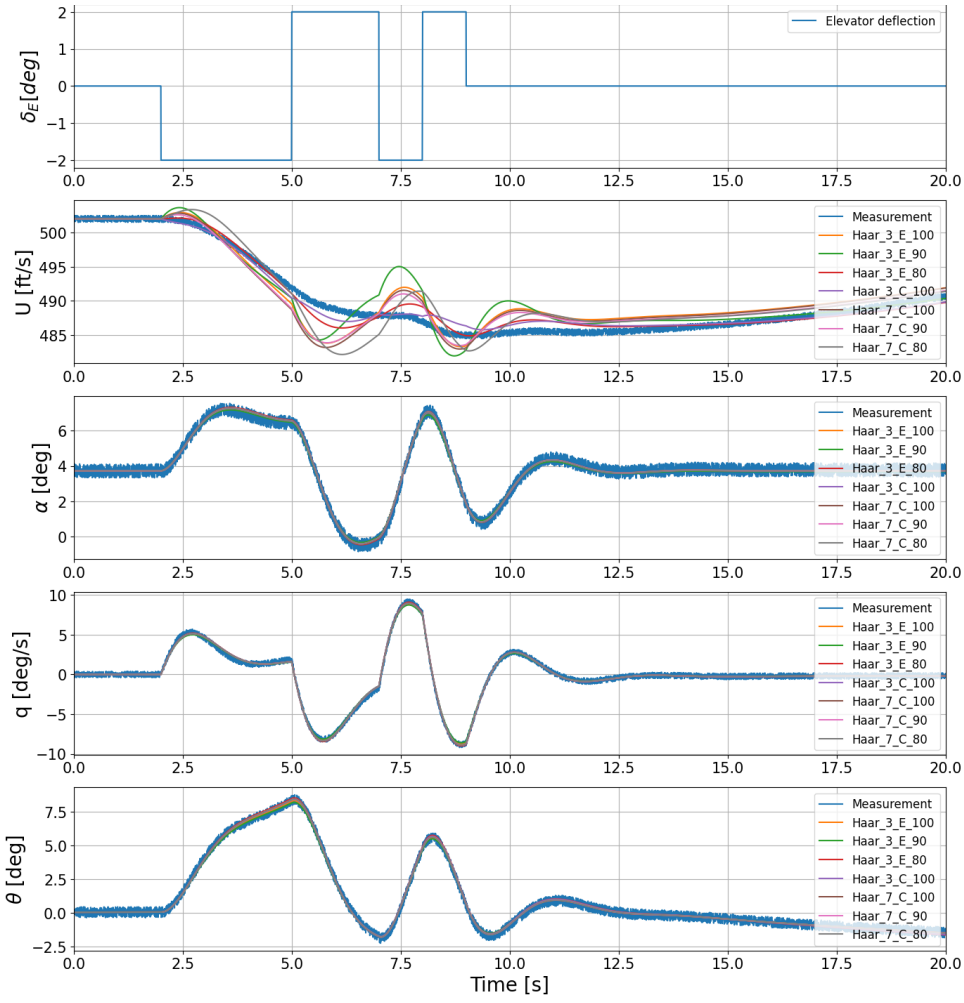

Fig. 6. Measurement data and responses of the linear models obtained as a result of the identification

Analyzing the charts in Fig. 7, it is evident that for some parameters, such as M_w, M_q and M_{dE}, all computational cases yielded similar estimates. On the other hand, there are significant discrepancies in the estimates between some identification cases, particularly for the derivatives X_w, X_q and X_{dE}. It is important to note that these parameters are used to determine the aircraft's longitudinal velocity U, for which the largest discrepancies between the identified models and the measurements were observed. Additionally, it is worth mentioning that these parameters mainly affect short-period oscillations. In such cases, it is advisable to use not only the 3-2-1-1 input signal for identification but also the 1-1 doublet signal with a switching time of less than one second to excite more short-period oscillations.

Table 3. Integrated differences between the measurement data (without measurement noise) and the responses of the identified linear models

Method	ϵ_U [ft]	ϵ_α[deg· s]	ϵ_q[deg]	ϵ_θ [deg· s]
Haar_3_E_100	34.408	1.235	1.412	0.878
Haar_3_E_90	30.611	1.833	1.837	1.476
Haar_3_E_80	14.605	1.145	1.647	1.787
Haar_3_C_100	12.994	1.249	1.529	1.496
Haar_7_C_100	34.518	1.172	1.350	0.856
Haar_7_C_90	29.503	1.170	1.369	0.961
Haar_7_C_80	31.770	1.247	1.377	0.953
Numerical linearization	14.875	1.349	2.577	4.279

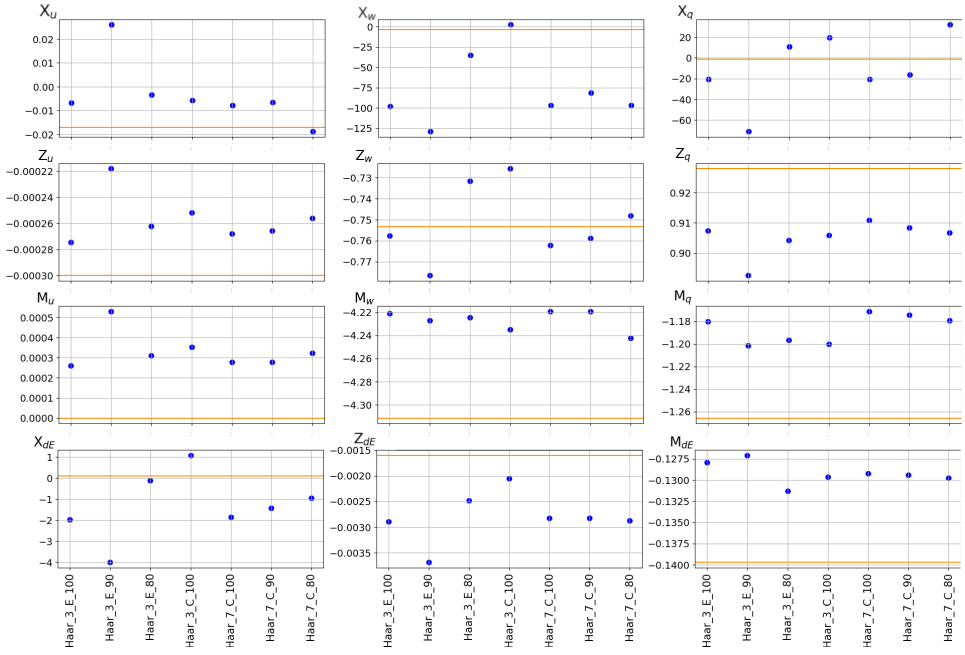

Fig. 7. Comparison of identified parameters for different computational cases (blue dots) with parameters obtained through numerical linearization (orange lines)

To compare the estimated parameter values between different computational cases, an additional coefficient ν_i was introduced, representing the sum of relative estimation errors for each computational case.

$$\nu_i = \frac{1}{N}\sum_{n=1}^{N}\frac{|\theta_i - \theta_{refi}|}{|\theta_{refi}|}, \tag{20}$$

where N denotes the number of identified model parameters.

The values for these coefficients for the various computational cases are summarized in Table 4.

Table 4. Comparison of the average relative sum of differences between the identified parameter values and the parameter values obtained through numerical linearization

Method	Value
Haar_3_E_100	5.55
Haar_3_E_90	11.98
Haar_3_E_80	2.02
Haar_3_C_100	2.68
Haar_7_C_100	5.42
Haar_7_C_90	4.40
Haar_7_C_80	5.68

The values in Table 4 indicate that the identification cases Haar_3_E_80, and Haar_3_C_100 achieved derivatives closest to the reference values. It is also worth noting that these are the cases with the smallest differences for velocity U. In the other cases, the differences are larger.

6. Conclusions

This study demonstrated that wavelet transforms can be successfully applied to identify the model parameters of an aircraft's longitudinal motion. This work is among the few studies exploring the use of wavelet transforms for this purpose, examining the impact of different decomposition levels and weighting functions on the identification results. Additionally, it introduced the application of a high-pass filter for wavelet transform coefficients, which has not been employed in other studies. The results obtained are comparable to, and in some cases even better than, those of models derived from numerical linearization. However, it is important to note that the calculations were conducted using artificially noised responses of a nonlinear aircraft motion model, focusing solely on decoupled longitudinal motion, which means the results could differ if real-world data were used.

The analysis revealed a positive impact from both the coherence-based weight function and higher levels of HPWC filtering, particularly in reducing the error for longitudinal velocity U, which proved to be the most challenging response to match. This difficulty likely stems from the inherent complexity of aligning the responses of a non-linear model with those of a linear model.

While increasing the decomposition level helped reduce the error for α, q, and θ, it did not improve the results for velocity U as expected. It was anticipated that a higher decomposition level combined with the coherence-based weight function would better suppress measurement noise and lead to significantly improved identification results.

Additionally, when using the coherence-based weight function with a higher decomposition level, the effect of the HPWC filter became less significant. This is likely because the combination of these methods was sufficient to minimize the impact of measurement noise. However, it is important to note that excessive filtering could distort the system's response, potentially worsening the identification results.

To improve the results, it is recommended to modify the input signal, such as incorporating a short-duration 1-1 doublet to more effectively excite the short-period dynamics of the system, or using multisine signals [33], which can generate a broader frequency spectrum in the system responses and potentially enhance signal coherence estimation. Additionally, the use of wavelet transforms for designing the input signal is worth exploring [19, 20]. Another possible modification could involve replacing the fully automated approach with a semi-automated one, where the person conducting the identification process has control over parameter adjustments when their values deviate from the expected range.

Additionally, replacing the linear model with a nonlinear model should be considered. Further improvement could also be achieved by experimenting with different levels of decomposition, weighting functions, wavelets, and filters for the coefficients obtained from the wavelet transform.

From a physical standpoint, applying a higher level of decomposition and assigning greater weights when determining the parameter change vector for components within the frequency range (0–2) Hz or eliminating other components might be beneficial. However, it should be noted that increasing the level of decomposition and the number of analyzed components significantly extends the computational time, as OEM is applied to each component separately. Also, important consideration is to change the sampling frequency. In this study, a high sampling frequency of 256 Hz was used. By lowering the sampling frequency, even through artificial downsampling, it would be possible to analyze more low-frequency bands at the same decomposition level. This would allow for a more detailed examination of low-frequency components while maintaining computational efficiency.

References

[1] L.A. Zadeh. From circuit theory to control theory. *Proceeding of the Institute of Radio Engineers*, 50(5):856–865, 1962. doi: 10.1109/JRPROC.1962.288302.

[2] Ravindra V. Jategaonkar. *Flight Vehicle System Identification: A Time-Domain Methodology*. American Institute of Aeronautics and Astronautics, Inc, Reston, VA, USA, 2015. doi: 10.2514/4.102790.

[3] M.J. Eklund and M.J. Korenberg. Simulation of aircraft pilot flight controls using nonlinear system identification. *Simulation*, 2000. doi: 10.1177/003754970007500201.

[4] H. Glauert. Analysis of phugoids obtained by a recording airspeed indicator. *Aeronautical Research Council, A.R.C R&M 576*, 1919.

[5] F.H. Norton. A study of longitudinal dynamic stability in flight, 1924. Raport: NACA-TR-170 url: https://ntrs.nasa.gov/citations/19930091236.

[6] M. Shinbort. A least squares curve fitting method with applications to the calculation of stability coefficients from transient-response data, 1951. Raport: NACA-TN-2341 url: https://ntrs.nasa.gov/citations/19930082980.

[7] K.l-J. Åström and B. Torsten. Numerical identification of linear dynamic systems from normal operating records. *IFAC Proceedings Volumes*, 2(2):96–111, 1965. doi: 10.1016/S1474-6670(17)69024-4.

[8] B. Ebrahimi and F. Barzamini. Aircraft system identification using parametric approaches and intelligent modeling. In *2021 IEEE Aerospace Conference (50100)*, pages 1–12, 2021. doi: 10.1109/AERO50100.2021.9438492.

[9] M. Jamil, M. Ahsan, M.J. Ahsan, and M. Choudhry. Time domain system identification of longitudinal dynamics of a uav: A grey box approach. In *International Conference on Emerging Technologies*, pages 1–6, 2015. doi: 10.1109/ICET.2015.7389200.

[10] P.G. Hamel and J. Kaletka. Advances in rotorcraft system identification. *Progress in Aerospace Sciences*, 33(3):259–284, 1997. doi: 10.1016/S0376-0421(96)00005-X.

[11] J.A. Grauer. Frequency response estimation for multiple aircraft control loops using orthogonal phase-optimized multisine inputs. *Processes*, 10(4), 2022. doi: 10.3390/pr10040619.

[12] M.B. Tischler and R.K. Remple. *Aircraft and Rotorcraft System Identification*. American Institute of Aeronautics and Astronautics, Reston, VA, USA, 2012. doi: 10.2514/4.868207.

[13] S.L. Brunton and J.N. Kutz. *Data-Driven Science and Engineering: Machine Learning, Dynamical Systems, and Control*. Cambridge University Press, Cambridge, England, 2019. doi: 10.1017/9781108380690.

[14] S.S. Kumari and V. Sadasivam. Wavelet-based base line wandering removal and R peak and QRS complex detection. *Internatinal Journal of Wavelets Multiresolution and Information Processing*, 05(06):927–939, 2007. doi: 10.1142/S0219691307002129.

[15] J.L.C.R. Vila, S.H.S. Carneiro, J.N.V. Goulart, C.T.M. Anflor, and A.B. Jorge. Wavelet-based numerical investigation on damage localisation and quantification in beams using static deflections and mode shapes. *European Journal of Mechanics - A/Solids*, 107:105351, 2024. doi: 10.1016/j.euromechsol.2024.105351.

[16] T. Ueda, M. Iio, and T. Ikeda. Flutter prediction using continuous wavelet transform. *Transactions of the Japan Society for Aeronautical and Space Sciences*, 51(174):275–281, 2009. doi: 10.2322/tjsass.51.275.

[17] P. Parihar, U. Kumar, D. Kaliyari, and K.N. Tk. Automatic maneuver detection in flight data using wavelet transform and deep learning algorithms. In *SAE Technical Paper 2024-26-0462*, 2024. doi: 10.4271/2024-26-0462.

[18] H.M. Paiva, R.K.H. Galvao, and T. Yoneyama. A wavelet band-limiting filter approach for fault detection in dynamic systems. *IEEE Transactions on Systems, Man, and Cybernetics - Part A: Systems and Humans*, 38(3):680–687, 2008. doi: 10.1109/TSMCA.2008.918593.

[19] P. Lichota, K. Sibilski, and P. Ohme. D-optimal simultaneous multistep excitations for aircraft parameter estimation. *Journal of Aircraft*, 54:747–758, 2017. doi: 10.2514/1.C033794.

[20] M. Roeser and N. Fezans. Method for designing multi-input system identification signals using a compact time-frequency representation. *CEAS Aeronautical Journal*, 12, 2021. doi: 10.1007/s13272-021-00499-6.

[21] P. Lichota. Wavelet transform-based aircraft system identification. *Journal of Guidance Control and Dynamics*, 46(2):350–361, 2023. doi: 10.2514/1.G006654.

[22] P. Lichota, M. Jacewicz, R. Głębocki, and D. Miedziński. Wavelet-based identification for spinning projectile with gasodynamic control aerodynamic coefficients determination. *Sensors*, 22(11):1–16, 2022. doi: 10.3390/s22114090.

[23] M. Naruoka, T. Hino, and T. Tsuchiya. Real-time system identification of aircraft dynamics using time-frequency wavelet analysis. In *27th Congress of the International Council of the Aeronautical Sciences 2010, ICAS 2010*, Nice, France, 2010.

[24] H.M. Paiva and R.K.H. Galvao. Wavelet-packet identification of dynamic systems in frequency subbands. *Signal Processing*, 86(8):2001–2008, 2006. doi: 10.1016/j.sigpro.2005.09.021.

[25] Y. Tan, X. Dang, F. Liang, and C-Y. Su. Dynamic wavelet neural network for nonlinear dynamic system identification. In *Proceedings of the 2000 IEEE International Conference on Control Applications*, pages 214–219, 2000. doi: 10.1109/CCA.2000.897426.

[26] E. Morelli. System identification programs for aircraft (SIDPAC). AIAA Atmospheric Flight Mechanics Conference. Monterey, CA, USA, 2002. doi: 10.2514/6.2002-4704.

[27] V. Klein and E.A. Morelli. *Aircraft System Identification: Theory and Practice*. American Institute of Aeronautics and Astronautics, Reston, VA, USA, 2006.

[28] M.V. Cook. *Flight Dynamics Principles: A Linear Systems Approach to Aircraft Stability and Control*. Butterworth-Heinemann, Burlington, MA, USA, 2007. doi: 10.1016/B978-0-7506-6927-6.X5000-4.

[29] M. Żugaj. *Układy automatycznego sterowania lotem (Automatic Flight Control Systems)*. Oficyna Wydawnicza Politechniki Warszawskiej, Warsaw, Poland, 2011. (in Polish).

[30] I. Daubechies. *Ten Lectures on Wavelets*. Society for Industrial and Applied Mathematics, University City Science Center Philadelphia, PA, USA, 1992.

[31] W. Rakowski. *Przekształcenia falkowe: aspekty obliczeniowe w praktyce inżynierskiej (Wavelet Transforms: Computational Aspects in Engineering Practice)*. Oficyna Wydawnicza Politechniki Białostockiej, Białystok, Poland, 2018. (in Polish).

[32] J. Thomas. Using the coherence function as a means to improve frequency domain least squares. Master's thesis, The Russ College of Engineering and Technology of Ohio University, Athens, OH, USA, 2007. url: https://api.semanticscholar.org/CorpusID:125283295.

[33] P. Young and R.J. Patton. Frequency domain identification of remotely-piloted helicopter dynamics using frequency-sweep and Schroeder-phased test signals. In *AIAA Atmospheric Flight Mechanics Conference*. American Institute of Aeronautics and Astronautics, 1988. doi: 10.2514/6.1988-4349.